# 8D.8 REGIONAL CLIMATE MODEL SIMULATION OF SUMMER RAINFALL OVER SOUTHEAST CHINA

Wan-Ru Huang*, Johnny C. L. Chan and Andie Au-Yeung
Guy Carpenter Asia-Pacific Climate Impact Centre, School of Energy and Environment,
City University of Hong Kong, Hong Kong, China

## 1. INTRODUCTION

The cumulus parameterization scheme has been identified as a key model component that affects the model's ability to simulate the diurnal cycle of regional rainfall. Although numerous cumulus parameterization schemes exist, none performs equally well under all conditions. It is therefore important to identify a suitable cumulus scheme for the model simulation for a particular area (e.g. Giorgi and Shields 1999). In this study, our focus is on the regional climate model simulation of the summer precipitation formation over Southeast China [i.e. SEC; (110$^o$E-118$^o$E, 21$^o$-25$^o$N) marked in Fig. 1], where the observational characteristics of diurnal variations of precipitation have been examined in detail (e.g. Huang et al. 2010; Huang and Chan 2011) but a suitable model simulation of these characteristics has not been made. The evaluation focuses on the sensitivity of the choice of cumulus parameterizations and model domain.

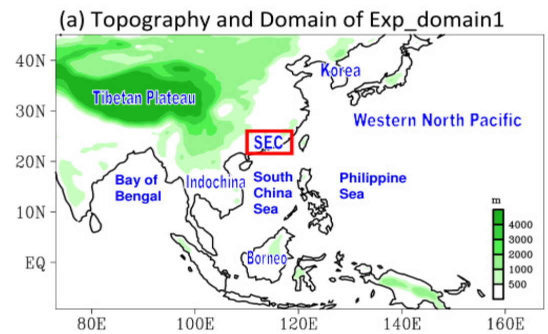


**Fig. 1** Topography and domain of the numerical simulations with the buffer zone excluded for Exp_domain1 listed in Table 1.

## 2. MODEL SETUP AND OBSERVATIONAL DATA

The model used here is the regional climate model version 3 (RegCM3), which has four available choices for the process of cumulus parameterizations. Two groups of experiments (see Table 1) are conducted in the present work to test the sensitivity of convective parameterization and domain choice. In Exp_domain1, a model domain covering the entire Tibetan Plateau (Fig. 1) is adopted with one of four available convective parameterization schemes: referred to EMU1, GFC1, GAS1 and AK1. In Exp_domain2, another model domain covering only the eastern part of the Tibetan Plateau is used and experiments are named as EMU2, GFC2, GAS2 and AK2. Other setups of model simulation, which remain the same for all experiments listed in Table 1, are described below.

**Table 1** Design of the sensitivity experiments

| Group of Experiments (Model Domain) | Individual Experiment | Convective Scheme | Closure |
|---|---|---|---|
| Exp_domain1 (73$^o$E-167$^o$E, 10$^o$S-45$^o$N) | EMU1 | MIT-Emanuel | – |
| | GFC1 | Grell | Fritsch-Chappell |
| | GAS1 | Grell | Arakawa-Schubert |
| | AK1 | Anthes-Kuo | – |
| Exp_domain2 (93$^o$E-167$^o$E, 10$^o$S-45$^o$N) | EMU2 | MIT-Emanuel | – |
| | GFC2 | Grell | Fritsch-Chappell |
| | GAS2 | Grell | Arakawa-Schubert |
| | AK2 | Anthes-Kuo | – |

This study chooses the BATS scheme to calculate the ocean fluxes. The sea surface temperature (SST) data uses the Optimum Interpolation SST V2 weekly mean data obtained from the Climate Diagnostics Center of the US National Oceanic and Atmospheric Administration. In addition, the 2.5$^o$×2.5$^o$, 6-h multiple level data from the European Centre for Medium-Range Weather Forecast 40 year (ERA40) reanalysis are used as the perfect boundary conditions for driving the RegCM3. These lateral boundary conditions are provided every 6 h via a relaxation method with a 15-grid buffer zone, following Chow and Chan (2009). The model used here has 20 vertical levels from surface level up to 10 hPa. The horizontal resolution is 60 km. Five years of simulations from 1998 to 2002 have been performed. In each simulation, the integration is from 1 May to 31 August.

Analysis of observational precipitation uses a 3-hourly, 0.5° longitude × 0.5° latitude gridded Tropical Rainfall Measuring Mission (TRMM) 3G68 2B31 precipitation dataset. For the examination of atmospheric conditions, meteorological variables are extracted from the 3-hourly GEOS5 (Goddard Earth Observing System Model Version 5) reanalysis dataset, following Huang and Chan (2011).

## 3. RESULTS

According to Huang and Chan (2011), the evolution of $P_{SEC}$ can be rewritten as:

$$P_{SEC} = \overline{P}_{SEC} + \Delta P_{SEC}$$
$$\cong \overline{P}_{SEC} + S1(P)_{SEC} + S2(P)_{SEC} \qquad (1)$$

where $\overline{P}_{SEC}$, $\Delta P_{SEC}$, $S1(P)_{SEC}$, and $S2(P)_{SEC}$ are the mean, anomalies, diurnal harmonic and semidiurnal harmonic of $P_{SEC}$ respectively. Because the characteristics of these components are very different

* *Corresponding author address:* Wan-Ru Huang, GCCC at City University of Hong Kong, e-mail: wrhuang@cityu.edu.hk

from each other, an acceptable model must be capable of simulating the temporal evolution of these components in order to be capable of simulating $P_{SEC}$. To demonstrate this hypothesis, all the ability of RegCM3 in simulating $\overline{P}_{SEC}$, $\Delta P_{SEC}$, $S1(P)_{SEC}$ and $S2(P)_{SEC}$ is evaluated in this study. Results of model simulations for Exp_domain1 are shown in Fig. 2.

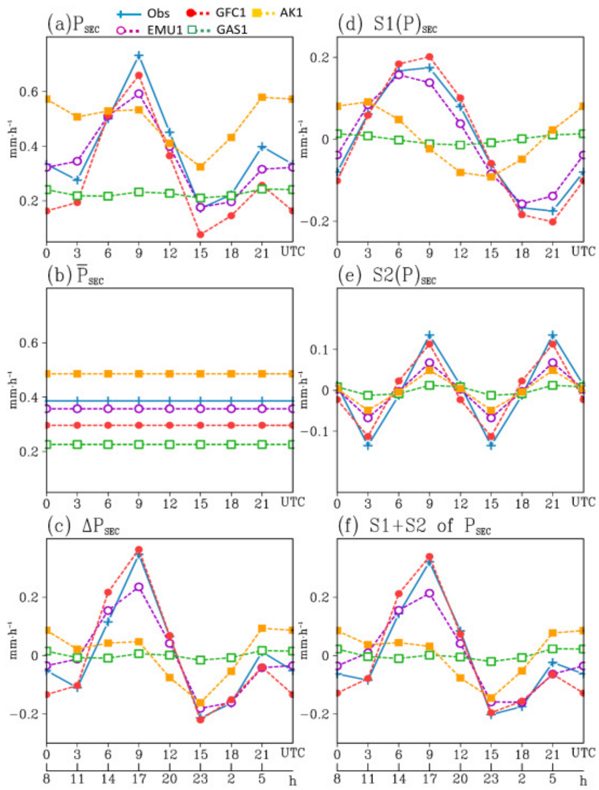


**Fig. 2** (a) The temporal evolution of 3-hourly $P_{SEC}$ averaged during 1998-2002 summers extracted from TRMM product and model simulations (including EMU1, GFC1, GAS1 and AK1 listed in Table 1). (b) to (f) respectively is the daily mean, the anomalies, the diurnal harmonic S1, the semi-diurnal harmonic S2 and (S1+S2) of $P_{SEC}$. The color legends are given in atop of (a).

Visually, the use of EMU1 and GFC1 is better than the use of GAS1 and AK1 for RegCM3 to simulate accurately the variation of $P_{SEC}$ (Fig. 2a). By separating $P_{SEC}$ into $\overline{P}_{SEC}$ (Fig. 2b) and $\Delta P_{SEC}$ (Fig. 2c) based on Eq. 1, it becomes even clearer that EMU1 is better than GFC1 for simulating $\overline{P}_{SEC}$, whereas the reverse is true for simulating $\Delta P_{SEC}$. Similar features are also revealed in Exp_domain2, as suggested by Table 2 that the GFC2 — with a higher Scorr, a higher Tcorr and a smaller RMSE for $\Delta P_{SEC}$ (see rows 4-6) — is more suitable than EMU2 in simulating the variations of $\Delta P_{SEC}$. Recall, the variability of $\Delta P_{SEC}$ can be approximately explained by the combination of $S1(P)_{SEC}$ and $S2(P)_{SEC}$ (e.g. Fig. 2f). As the $S1(P)_{SEC}$ and $S2(P)_{SEC}$ have different temporal evolutions (e.g. Figs. 2d-e), we further examine the ability of the model in simulating $S1(P)_{SEC}$ and $S2(P)_{SEC}$ to understand why GFC1 gives a better simulation of the variation of $\Delta P_{SEC}$ than the other schemes.

**Table 2** Selected statistical variables for measuring the ability of model in simulating different components of precipitation formation over the domain of SEC. The smallest value of RMSE (i.e. root-mean-square error) and the Scorr (spatial correlation coefficient), as well as Tcorr (temporal correlation coefficient), exceeding the 95% confidence level is in bold

| Comp. | Field \ Obs vs. Simulations | Obs | EMU1 | GFC1 | GAS1 | AK1 | EMU2 | GFC2 | GAS2 | AK2 |
|---|---|---|---|---|---|---|---|---|---|---|
| $\overline{P}$ | Value (unit: $mmh^{-1}$) | 0.39 | 0.37 | 0.31 | 0.22 | 0.48 | 0.43 | 0.19 | 0.31 | 0.30 |
| | Scorr | | **0.52** | 0.44 | 0.35 | 0.46 | 0.41 | 0.28 | 0.32 | 0.38 |
| | RMSE (unit: $mmh^{-1}$) | | **0.09** | 0.11 | 0.15 | 0.14 | 0.11 | 0.22 | 0.18 | 0.16 |
| $\Delta P$ | Tcorr | | **0.82** | **0.90** | 0.15 | 0.43 | **0.61** | **0.76** | 0.11 | 0.38 |
| | Scorr at 09 UTC | | 0.54 | **0.91** | 0.12 | -0.07 | 0.47 | **0.62** | 0.05 | -0.03 |
| | RMSE at 09 UTC (unit: $mmh^{-1}$) | | 0.28 | **0.14** | 0.47 | 0.45 | 0.46 | 0.41 | 0.60 | 0.59 |
| S1 | Var[S1(P)]/Var[$\Delta P$] (unit: %) | 64.8 | 75.1 | 69.7 | 44.9 | 73.5 | 72.4 | 57.7 | 61.6 | 72.7 |
| | Amplitude (unit: $mmh^{-1}$) | 0.19 | 0.16 | 0.20 | 0.02 | 0.08 | 0.22 | 0.17 | 0.03 | 0.09 |
| | Tcorr | | **0.87** | **0.93** | -0.54 | -0.10 | **0.66** | **0.78** | -0.15 | -0.34 |
| | Scorr at 09 UTC | | 0.49 | **0.93** | -0.61 | -0.14 | 0.33 | **0.86** | -0.14 | -0.02 |
| | RMSE at 09UTC (unit: $mmh^{-1}$) | | 0.24 | **0.12** | 0.41 | 0.43 | 0.35 | 0.32 | 0.42 | 0.45 |
| S2 | Var[S2(P)]/Var[$\Delta P$] (unit: %) | 31.1 | 18.9 | 26.2 | 48.1 | 21.4 | 24.3 | 30.3 | 28.5 | 21.2 |
| | Amplitude (unit: $mmh^{-1}$) | 0.13 | 0.07 | 0.12 | 0.01 | 0.05 | 0.08 | 0.11 | 0.01 | 0.04 |
| | Tcorr | | **0.94** | **0.90** | **0.82** | **0.91** | **0.68** | **0.73** | **0.62** | **0.69** |
| | Scorr at 09 UTC | | **0.63** | **0.84** | **0.65** | **0.64** | **0.54** | **0.65** | **0.51** | **0.52** |
| | RMSE at 09 UTC (unit: $mmh^{-1}$) | | 0.03 | **0.02** | 0.04 | 0.03 | 0.11 | 0.09 | 0.18 | 0.14 |

As seen from Fig. 2d, both the amplitude and the phase evolution of the observed $S1(P)_{SEC}$, which has maximum values at 1700 h/0900 UTC (Huang and Chan 2011), can be well captured by the simulation using GFC1. For the EMU1-simulated $S1(P)_{SEC}$, its phase evolution is also similar to the observation but the amplitude is weaker. In contrast, GAS1 and AK1 have problems to simulate realistically the amplitude and phase evolution of $S1(P)_{SEC}$. These increases of errors in simulating $S1(P)_{SEC}$ due to the change of cumulus schemes are also revealed in Exp_domain2, showing that the Tcorr between observed and simulated $S1(P)_{SEC}$ is much smaller in GAS2 and AK2 than in GFC2 and EMU2 (see Table 2). This finding is consistent with Zanis et al. (2009) suggesting that GAS generally displays a weaker diurnal variation than GFC because the GAS scheme is invoked mainly at times when the SUBEX scheme is also invoked due to major weather systems.

Further, Table 2 for $S1(P)_{SEC}$ shows smaller Tcorr, smaller Scorr and larger RMSE in Exp_domain1 than in Exp_domain2, confirming again that the choice of model domain covering the entire Tibetan Plateau for simulation can improve the ability of the model in simulating the diurnal rainfall formation over SEC. On the other hand, as seen from Fig. 2e and Tcorr in Table 2 for $S2(P)_{SEC}$, all schemes are found to be capable of realistically simulating the phase evolution of $S2(P)_{SEC}$, while GFC1 is more accurate than other schemes in representing the amplitude of $S2(P)_{SEC}$. In other words, a scheme with the best performance on the evolution of $S1(P)_{SEC}$ and $S2(P)_{SEC}$ also has the best performance on $\Delta P_{SEC}$.

Numerous studies have suggested that the change of moisture flux convergence is one of the major factors that affect the formation of precipitation over East Asia (e.g. Chen 2005; Huang et al. 2010). Likely, the scheme which performs best on the formation of precipitation is due to its better performance on the moisture flux convergence. To verify this hypothesis, we examine the ability of the model in simulating the moisture supply for the formation of precipitation through diagnosing the following water vapor budget equation:

$$P = E + (-\nabla \bullet \mathbf{Q}) + (-\frac{\partial W}{\partial t}), \qquad (2)$$

where $W$, ($-\nabla\bullet\mathbf{Q}$), P and E are respectively the total precipitable water, the convergence of the vertical-integrated water vapor flux, the precipitation and the evaporation. Chen (2005) examined Eq. (2) and pointed out that the contributions of E and ($-\partial W/\partial t$) are much smaller than that of ($-\nabla\bullet\mathbf{Q}$) to the summer mean precipitation formation over East Asia [i.e. $\overline{P}$ ~ ($-\nabla\bullet\overline{\mathbf{Q}}$)]. Consistent with Chen (2005), the moisture flux convergence into SEC is responsible for the formation of $\overline{P}_{SEC}$ (Fig. 3). Among all the experiments, EMU1 not only gives a value of $(-\nabla\bullet\overline{\mathbf{Q}})_{SEC}$ closer to the observation, but also has a spatial distribution closer to the observed $(-\nabla\bullet\overline{\mathbf{Q}})_{SEC}$ (see also Table 3). As EMU1 performs best in the simulation of $(-\nabla\bullet\overline{\mathbf{Q}})_{SEC}$, it also performs best in the simulation of $\overline{P}_{SEC}$.

**Table 3** Statistical variables for measuring the ability of model in simulating different components of mositure flux convergence (-∇•Q) over the domain of SEC. The values of Scorr exceeding the 95% confidence level as well as the smallest value of RMSE between the simulated and observed patterns are emphasized with bold type

| Comp. | Field \ Simulations | EMU1 | GFC1 | GAS1 | AK1 | EMU2 | GFC2 | GAS2 | AK2 |
|---|---|---|---|---|---|---|---|---|---|
| Mean | [-∇•Q(model)] / [-∇•Q(obs)] | 0.95 | 0.79 | 0.56 | 1.23 | 1.13 | 0.49 | 0.79 | 0.75 |
| | Scorr | **0.61** | 0.47 | 0.32 | 0.48 | 0.39 | 0.32 | 0.28 | 0.35 |
| | RMSE (unit: $mmh^{-1}$) | **0.11** | 0.14 | 0.18 | 0.21 | 0.14 | 0.25 | 0.16 | 0.16 |
| S1 | Var[-∇•Q(model)]/Var[-∇•Q(obs)] | 0.78 | **1.11** | 0.10 | 0.35 | 1.34 | 0.85 | 0.21 | 0.46 |
| | Scorr at 09 UTC | **0.51** | **0.90** | -0.58 | -0.23 | 0.31 | **0.72** | -0.21 | -0.10 |
| | RMSE at 09 UTC (unit: $mmh^{-1}$) | 0.23 | **0.13** | 0.41 | 0.45 | 0.37 | 0.31 | 0.44 | 0.48 |
| S2 | Var[-∇•Q(model)]/Var[-∇•Q(obs)] | 0.35 | **0.91** | 0.06 | 0.19 | 0.54 | 0.80 | 0.07 | 0.13 |
| | Scorr at 09 UTC | **0.65** | **0.80** | **0.64** | **0.63** | **0.57** | **0.64** | 0.43 | 0.44 |
| | RMSE at 09 UTC (unit: $mmh^{-1}$) | 0.04 | **0.02** | 0.05 | 0.04 | 0.12 | 0.10 | 0.19 | 0.13 |

For the maintenance of S1(P) over SEC, Huang et al. (2010) pointed out that the S1 of wind convergence change can induce more moisture convergence into SEC to support its maximum precipitation, i.e. $S1(P)_{SEC}$ ~$S1(-\nabla\bullet\mathbf{Q})_{SEC}$, occurring at 1700 h/0900 UTC. It is noted from Table 3 that for a particular scheme, its ability on the simulation of $S1(-\nabla\bullet\mathbf{Q})_{SEC}$ is better in Exp_domain1 than in Exp_domain2, consistent with what has been found in Table 2 for the simulation of $S1(P)_{SEC}$. In addition, without a change in the model domain, GFC performs best (while EMU ranks in the second place) among the four schemes in the simulation of $S1(-\nabla\bullet\mathbf{Q})_{SEC}$. Additional information to explain this feature can be obtained from Fig. 4 showing the diurnal circulation and its related water vapor convergence at 1700 h/0900 UTC [i.e. the timing of maximum observed $S1(P)_{SEC}$] for observation and Exp_domain1.

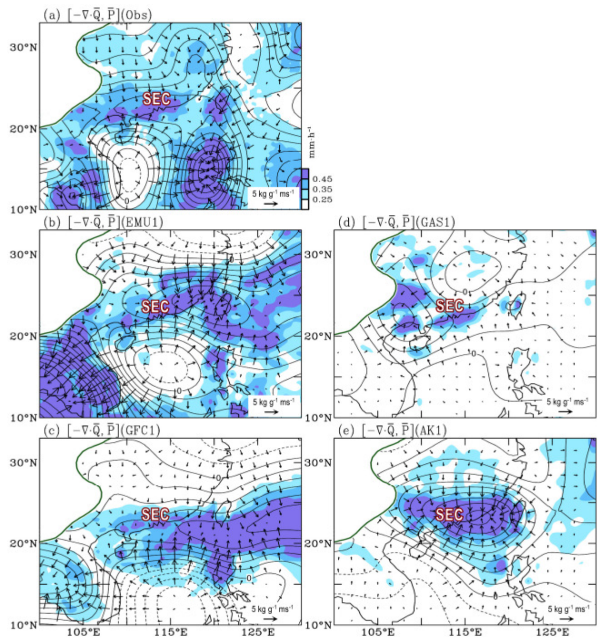


**Fig. 3** (a) The mean of observational water vapor flux convergence [($-\nabla\bullet\overline{\mathbf{Q}}$); contours] and precipitation ($\overline{P}$; shadings) during the 1998-2002 summer periods. The vectors of the convergence of water vapour flux are also added in (a). (b) to (e) is similar to (a), but for the model simulation extracted from EMU1, GFC1, GAS1 and AK1 experiment respectively. The color scale of $\overline{P}$ is given in right bottom of (a) and the contour interval of ($-\nabla\bullet\overline{\mathbf{Q}}$) is $8 \times 10^{-2}$ mm $h^{-1}$. The location of SEC is added in (a)-(e) and the mountain areas located left of the green line are blocked.

It is noted that although all schemes are capable of simulating the sea breeze circulation, their related vertical motions are not always in the right position as compared to the observed one (Figs. 4a-e). For example, GAS1 and AK1-simulated upward motions at 0900 UTC are shifted westward to inner China. Such model biases on the simulation of diurnal atmospheric circulation would result in downward motion, which is originally located over the ocean areas, to shift westward to SEC. This westward shift of diurnal circulation would further result in the divergence of moisture flux occurring over SEC [see negative $S1(-\nabla\bullet\mathbf{Q})_{SEC}$ in Figs. 4f-j and negative Scorr of $S1(-\nabla\bullet\mathbf{Q})_{SEC}$ in Table 3]. As a consequence, the GAS1 and AK1-simulated $S1(P)_{SEC}$ is suppressed at 1700 h/0900 UTC, which explains why GAS1 and AK1 tend to have larger biases in the simulation of the timing of $S1(P)_{SEC}$. For GFC1 and EMU1, which perform better in simulating both the diurnal atmospheric circulation and moisture flux convergence over SEC, they have more accurate simulations on $S1(P)_{SEC}$.

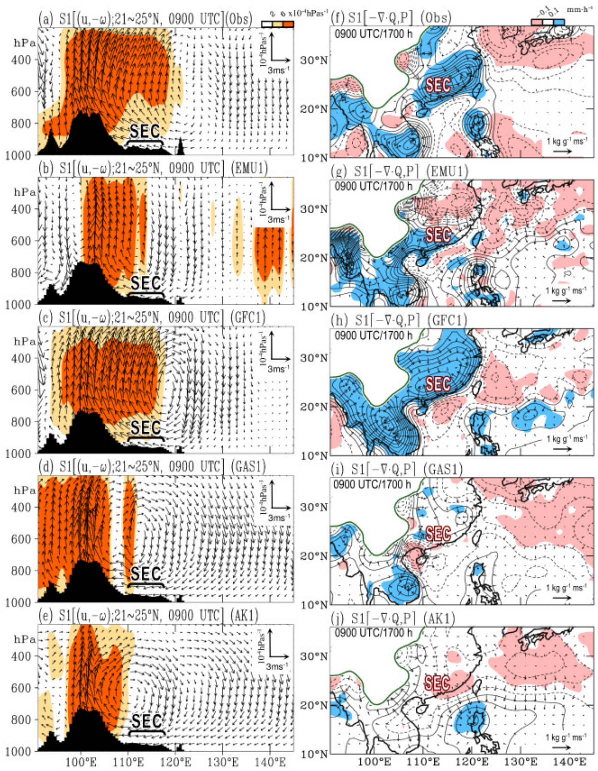


**Fig. 4** (a) The observed vertical cross-section of diurnal harmonic of vertical velocity [i.e. S1(-ω); shadings] superimposed with [S1(u, -ω); vector] averaged between $21^{o}$-$25^{o}$N at 0900 UTC (i.e. 1700 h for SEC) for the 1998-2002 summer periods. (b) to (e) is similar to (a), but for the simulated results of EMU1, GFC1, GAS1 and AK1 respectively. (f)-(j) correspond to (a)-(e), but for the $S1(-\nabla\bullet\mathbf{Q})$ (contours) superimposed with S1(P) (shadings) at 0900 UTC. The color scale S1(-ω) in (a)-(e) is given in atop of (a) and the color scale of S1(P) in (f)-(j) is given in atop of (f). The contour interval of $S1(-\nabla\bullet\mathbf{Q})$ in (f)-(j) is $3\times10^{-2}$ mm $h^{-1}$.

As for $S2(-\nabla\bullet\mathbf{Q})_{SEC}$, it is found in Table 3 that the choice of domain size covering only eastern Tibetan Plateau increases the model errors in simulating the $S2(-\nabla\bullet\mathbf{Q})_{SEC}$. Huang and Chan (2011) demonstrated that the variation of $S2(P)_{SEC}$ is also mainly controlled by the variation of $S2(-\nabla\bullet\mathbf{Q})_{SEC}$. Consistent with Huang and Chan (2011), an examination on the spatial distribution of $S2(-\nabla\bullet\mathbf{Q})_{SEC}$ in Exp_domain1 at 0900 UTC [i.e. one of the timing of the occurrence of maximum $S2(P)_{SEC}$] indicates that all schemes are capable of capturing the feature of S2 of moisture flux convergence into SEC to supply the maximum of $S2(P)_{SEC}$ (not shown). This explains why all schemes are capable of depicting the phase evolution of $S2(P)_{SEC}$ (see Fig. 2e). Most importantly, features shown in these examinations demonstrate that an accurate representation of the moisture convergence is critical in the simulation of $P_{SEC}$.

**4. SUMMARY**

In this study, the capability of RegCM3 in simulating the summer precipitation over East Asia, with focus on diurnal variations of precipitation over Southeast China (SEC), is evaluated. Results show that the Emanuel cumulus scheme has a more realistic simulation of summer mean rainfall in East Asia, while the GFC (Grell scheme with the Frisch-Chappell convective closure assumption) scheme is better in simulating the diurnal variations of rainfall over Southeast China. The better performance of these two schemes [relative to the other two schemes in RegCM3: the Kuo scheme and the GAS (Grell scheme with the Arakawa–Schubert closure assumption) scheme] is found to be attributable to the reasonable reproduction of the major formation mechanism of rainfall — the moisture flux convergence — over East Asia and Southeast China. Furthermore, when the simulation domain covers the entire Tibetan Plateau, the diurnal variations of rainfall over Southeast China are found to exhibit a noticeable improvement without changes in the physics schemes. Further details can be found in Huang et al. (2012).

**References:**


Chen, T.-C., 2005: Variation of the Asian monsoon water vapor budget: interaction with the global-scale Modes. In: B. Wang (ed) The Asian Monsoon, Spring Verlag, pp 417-458

Chow, K.-C., and Chan J.C.L., 2009: Diurnal variations of circulation and precipitation in the vicinity of the Tibetan Plateau in early summer. *Climate Dynamics,* 32(1), 55-73.

Giorgi, F. and Shields C., 1999: Tests of precipitation parameterizations available in latest version of NCAR regional climate model (RegCM) over continental United States. *J. Geophys. Res.,* 104, 6353–6375.

Huang, W.-R., Chan J.C.L., and Wang S.-Y., 2010: A planetary-scale land–sea breeze circulation in East Asia and the western North Pacific. *Q. J. R. Meteorol. Soc*., 136, 1543–1553.

Huang, W.-R. and Chan J.C.L., 2011: Maintenance mechanisms for the early-morning maximum summer rainfall over Southeast China. *Q. J. R. Meteorol. Soc*., 137, 959–968.

Huang, W.-R., Chan J.C.L., and Au-Yeung A., 2012: Regional Climate Simulations of Summer Diurnal Rainfall Variations over East Asia and Southeast China (submitted to *Climate Dynamics*)

Zanis P., Douvis C., Kapsomenakis I., Kioutsioukis I., Melas D., and Pal J.S., 2009: A sensitivity study of the Regional Climate Model (RegCM3) to the convective scheme with emphasis in central eastern and southeastern Europe. *Theor. Appl. Climatol*., 97(3), 327-337.